Journal of Nuclear Materials 406 (2010) 7–18

Contents lists available at ScienceDirect

Journal of Nuclear Materials

journal homepage: www.elsevier.com/locate/jnucmat

Ab initio calculations and interatomic potentials for iron and iron alloys: Achievements within the Perfect Project

L. Malerba [a,*], G.J. Ackland [b], C.S. Becquart [c], G. Bonny [a], C. Domain [d], S.L. Dudarev [e], C.-C. Fu [f], D. Hepburn [b], M.C. Marinica [f], P. Olsson [d], R.C. Pasianot [g,h], J.M. Raulot [i], F. Soisson [f], D. Terentyev [a], E. Vincent [c,d,1], F. Willaime [f]

[a] *Structural Materials Group, Institute of Nuclear Materials Science, SCK-CEN, Boeretang 200, B-2400 Mol, Belgium*
[b] *School of Physics, CSEC and SUPA, The University of Edinburgh, Mayfield Road, Edinburgh EH9 3JZ, UK*
[c] *Unité de Matériaux et Techniques, UMR 8207, Université Lille-1, F-59655 Villeneuve d'Ascq Cédex, France*
[d] *Dept. MMC, EDF-R&D, Site des Renardières, F-77218 Moret-sur-Loing, France*
[e] *EURATOM/UKAEA Fusion Association, Culham Science Centre, Oxfordshire OX14 3DB, UK*
[f] *CEA, DEN, Service de Recherches de Métallurgie Physique, F- 91191 Gif-sur-Yvette, France*
[g] *CAC-CNEA, Depto. de Materiales, Avda. Gral. Paz 1499, 1650 San Martín, Pcia. Buenos Aires, Argentina*
[h] *CONICET, Avda. Rivadavia 1917, 1033 Buenos Aires, Argentina*
[i] *Institut Supérieur de Génie Mécanique et Productique (ISGMP), UMR CNRS 7078, Bat. B, Ile du Saulcy, F57045 Metz, Cedex 1, France*

A B S T R A C T

The objective of the FP6 Perfect Project was to develop a first example of integrated multiscale computational models, capable of describing the effects of irradiation in nuclear reactor components, namely vessel and internals. The use of *ab initio* techniques to study, in the most reliable way currently possible, atomic-level interactions between species and defects, and the transfer of this knowledge to interatomic potentials, of use for large scale dynamic simulations, lie at the core of this effort. The target materials of the Project were bainitic steels (vessel) and austenitic steels (internals), i.e. iron alloys. In this article, the advances made *within the Project* in the understanding of defect properties in Fe alloys, by means of *ab initio* calculations, and in the development of interatomic potentials for Fe and Fe alloys are overviewed, thereby providing a reference basis for further progress in the field. Emphasis is put in showing how the produced data have enhanced our level of understanding of microstructural processes occurring under irradiation in model alloys and steels used in existing nuclear power plants.

1. Introduction

Ab initio calculations based on density functional theory (DFT) can provide reliable data on energies and configurations of point-defects and solute/point-defect complexes in, for example, Fe alloys. These data can provide keys for the understanding of radiation damage production and evolution in steels for nuclear applications and are invariably needed to parameterise larger-scale models, aimed at predicting the microstructure evolution of these materials under irradiation. Thus, these types of calculations lie at the core of the effort of developing integrated multiscale computational models, capable of describing the effects of irradiation in nuclear reactor components, which was the objective of the 6th framework programme (FP6) Perfect Project (henceforth simply *the Project*). Yet, *ab initio* methods can be reasonably applied only to systems containing at the most hundreds of atoms. In order to study the evolution of large enough systems up to length- and time-scales comparable with those accessible in experiments, the use of semi-empirical interatomic potentials (hereafter simply *potentials*) currently remains a largely obligatory choice. Two objectives were therefore set since the beginning of the Project and delegated to a specific work-package: (i) to build an extended database of *ab initio* calculation results, consisting of point-defect and point-defect complex formation, binding and migration energies in Fe, including interaction with major substitutional (e.g. Cu, Ni, Mn, Si and P in the case of reactor pressure vessel – RPV – steels) and interstitial (e.g. C and N) alloying elements, or elements produced under irradiation by transmutation (e.g. He in austenitic steels); and (ii) to transfer this type of information, together with experimental data, via adequate formalisms and fitting procedures, into advanced potentials, capable of grasping the complexity of radiation damage in Fe alloys, including convenient descriptions of complex point-defect configurations, magnetism, thermodynamic driving forces etc., and ready for use in large-scale molecular dynamics (MD) or kinetic Monte Carlo (KMC) simulation

* Corresponding author. Tel.: +32 14 333090; fax: +32 14 321216.
E-mail address: lmalerba@sckcen.be (L. Malerba).
[1] Present address: AREVA NP, Centre Technique, Dept. Corrosion-Chimie, 30 Boulevard de l'Industrie, Espace Magenta, BP 181, 71205 Le Creusot Cedex, France.

0022-3115/$ - see front matter © 2010 Elsevier B.V. All rights reserved.
doi:10.1016/j.jnucmat.2010.05.016

techniques. The present article overviews the results obtained *by the Project* within this scope, while emphasising how the produced data have enhanced our level of understanding of microstructural processes occurring under irradiation in model alloys and steels used in existing nuclear power plants. It does not have, however, by any means the ambition of reviewing all literature results on the subject. It will be divided into three main parts: *ab initio* calculations (Section 2), development of advanced potentials for Fe (Section 3) and development of advanced potentials for Fe alloys (Section 4). In Section 5 a short summary and some concluding remarks, including a brief discussion of the outlook, are provided.

2. *Ab initio* calculations

A host of *ab initio* studies of Fe and Fe alloys have been performed, using different methods and approximations, in the course of the Project [1–17]. They can be organised in two groups: (i) study of point-defects (self-interstitial atoms – SIA – and vacancies) and point-defect clusters in pure α-Fe, to obtain configurations, formation energies and migration energies and mechanisms [1,4,6,8,16]; and (ii) study of the interaction of both substitutional (Cu, Mn, Ni, Si, P) [1,2,5,7,10–15] and interstitial (C, N) [3,17] alloying elements in α-Fe with single point-defects. In addition, calculations have been started devoted to, on the one hand, the interaction of small SIA clusters with C atoms [21] and, on the other, austenitic alloys, represented by Ni containing Fe and Cr impurities, focusing on the effect of He in stabilising small cavities [22].

The calculations performed with the Spanish Initiative for Electronic Simulations with Thousands of Atoms (SIESTA), code that are reported here based on the DFT, in the generalized gradient approximation (GGA) for exchange and correlation, using the Perdew–Burke–Enzerhof parameterisation [23], and spin polarised when applied to Fe. They make use of non-local norm-conserving pseudopotentials to represent the ionic core electrons, while valence electrons are described by linear combinations of numerical, localized, pseudo-atomic orbitals, which enable the code to work fast [18], but advise the first results to be validated by comparison with those obtained using more robust, plane-wave basis sets. The calculations performed within the Project were generally conducted at zero pressure (all the atomic forces and the components of the stress tensor set to zero), including full ionic relaxation.

The Vienna *Ab initio* Simulation Package (VASP) code [19,20], on the other hand, is a DFT plane-wave based code. The calculations performed with this code and reported here also use the GGA (Perdew et al. parameterisation [24]) for exchange and correlation and are spin polarised when applied to the study of Fe and Ni. For most calculations hitherto performed within the Project, fully non-local Vanderbilt-type ultrasoft pseudopotentials (USPP) were used to replace ionic core electrons [25]; more recently, the more accurate projector-augmented wave (PAW) method [26], with Vosko–Wilk–Nusair interpolation of the correlation potential [27], has been used instead.

In all cases, a supercell approach was used, with periodic boundary conditions at constant volume (VASP calculations), i.e. relaxing only the atomic positions in a supercell dimensioned with the equilibrium lattice parameter for Fe, or at constant pressure (SIESTA calculations).

2.1. Point defects and their clusters in α-Fe

Single point-defects in bcc-Fe have been studied both with VASP [1,2] and with SIESTA [4,6,8]. The results agree qualitatively, and generally also quantitatively; in particular, the relative stability of the ⟨1 1 1⟩ crowdion versus the ⟨1 1 0⟩ dumbbell (∼0.7 eV difference in energy) and the formation and migration energy of the single vacancy (∼0.65 eV) must be considered robust results.

According to calculations with SIESTA in 128 and 250 atom simulation boxes, SIA clusters in their ground state (0 K) are collections of parallel ⟨1 1 1⟩ crowdions starting from five SIA, while below this size they are collections of parallel ⟨1 1 0⟩ dumbbells [4,6,8]. This picture has been now partially challenged after the discovery, first suggested by empirical interatomic potentials [28], of the stability of non-parallel SIA cluster configurations, i.e. configurations where the dumbbells are not parallel to each other [16]. These non-parallel configurations (NPC), according to VASP calculations using the PAW method, which is deemed to be the most accurate in magnetic systems, appear to be the real ground state, or to be at least degenerate with stable ⟨1 1 0⟩ parallel-dumbbell configurations [16]. Moreover, empirical potential studies suggest them to be further stabilised at high temperature, as a consequence of their high formation entropy compared to the canonical configurations [16]. The NPC for clusters of two, three and four SIAs, together with the corresponding ⟨1 1 0⟩ parallel configurations, are pictorially shown in Fig. 1.

DFT also confirms that the main migration mechanism for the single SIA (dumbbell) involves concomitant translation and rotation to a different ⟨1 1 0⟩ direction, as proposed in 1964 by Johnson [29] (Fig. 2) [4,6,8], at variance with the mechanism based on the possibility of on-site rotation to ⟨1 1 1⟩ crowdion and subsequent glide, that was accepted a few years ago on the basis of early interatomic potential indications [30]. The migration energy is found to be 0.34 eV, in reasonable agreement with experimental measurements suggesting ∼0.3 eV [31]. The migration energies for di- and tri-interstitial clusters (so long as they stay in parallel configurations) have been determined to be around ∼0.4 eV, in

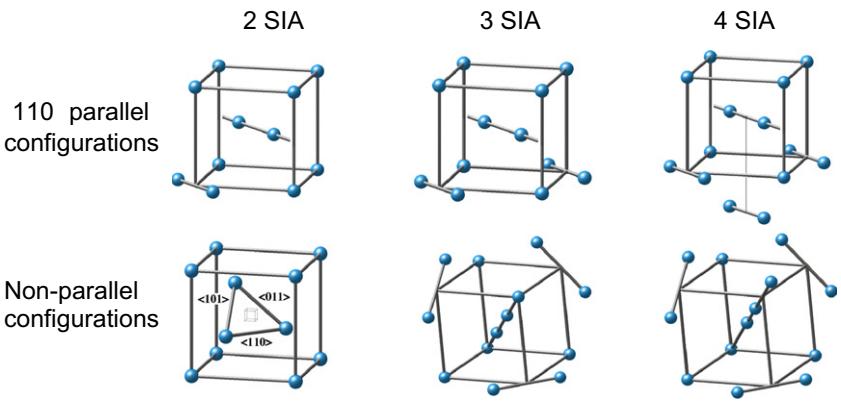

Fig. 1. Pictorial representation of stable ⟨1 1 0⟩ parallel (above) and non-parallel (below) configurations of small SIA clusters in bcc-Fe.

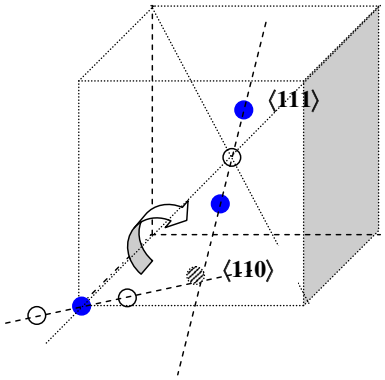

Fig. 2. Schematic representation of Johnson's mechanism for dumbbell migration (white circles, initial configuration; blue circles, final configuration; striped circle, atom at saddle point). (For interpretation of the references to colour in this figure legend, the reader is referred to the web version of this article.)

broad agreement with indications from resistivity recovery studies [4,6,8]. The impact of the stability of NPC, especially at high temperature, on the effective migration energy of SIA clusters, remains, however, yet to be properly quantified [16].

Concerning vacancy clusters, static DFT calculations confirm that the most stable configuration of the di-vacancy corresponds to two 2nd nearest neighbour (2nn) vacancies [2] and has a migration energy close to that of the single vacancy, while tri- and quadri-vacancies exhibit a lower migration energy, comparable with the migration energy of small SIA clusters [6,8]. Still, calculations within an atomistic kinetic Monte Carlo (AKMC) model, based on barriers obtained from DFT calculations with VASP, suggest that the migration energy of the di-vacancy may be somewhat lower than for the single-vacancy [32], as a consequence of a counter-intuitive mechanism, whereby the di-vacancy alternates a 2nn to a 4nn configuration, differently from the 2nn–1nn migration path assumed in the *ab initio* static calculations [33]. It is, however, noteworthy that static *ab initio* calculations and AKMC calculations with a Mendelev-type interatomic potential [34,35] provide similar values in the case of tri- and quadri-vacancies [32].

An extended compilation of *ab initio* results concerning point-defects and their clusters in pure Fe is provided in [36].

Table 1
Solute–solute binding energies (in eV) in first (1nn) and second (2nn) nearest neighbour determined by VASP/USPP *ab initio* calculations with 128 atom supercells and 27 *k* points. The Mn always stabilises in an antiferromagnetic state (data from [11]).

Case	Cu	Ni	Mn	Si
E_b (Cu–X 1nn)	0.16	0.02	0.02	0.06
E_b (Cu–X 2nn)	0.05	−0.01	−0.07	−0.05
E_b (Ni–X 1nn)		−0.10	−0.12	0.00
E_b (Ni–X 2nn)		−0.02	−0.12	−0.12
E_b (Mn–X 1nn)			−0.20	−0.03
E_b (Mn–X 2nn)			−0.18	−0.36
E_b (Si–X 1nn)				−0.32
E_b (Si–X 2nn)				−0.18

Table 2
Vacancy – solute binding energies (in eV) determined by VASP/USPP *ab initio* calculations with 128 atom supercells and 27 *k* points. For the Mn, the state is antiferro-magnetic. The results of the calculations are compared with available experimental data (data from [11]).

Case	Cu	Ni	Mn	Si	P
E_b (V–X 1nn)	0.16	0.03	0.10	0.25	0.32
E_b (V–X 2nn)	0.21	0.17	0.08	0.15	0.28
Exp.	0.11[a]	0.21[a]	0.15[b]	0.21[a]	//
	0.14[b]	0.22[b]		0.23[b]	

[a] Ref. [37].
[b] Ref. [38].

2.2. Solute atoms/point-defect interaction in α-Fe

2.2.1. Substitutional solute atoms

The study of the interaction of Cu, Ni, Mn and Si substitutional impurities with each other and with point-defects (the latter also for P) in the Fe matrix, performed with VASP [2,5,7,10,11,15] (also with SIESTA in the case of Cu and P [12–14]), provided numbers broadly consistent with the expected thermodynamic behaviour of these elements and with experimental assessments of point-defect/solute binding energies in bcc-Fe (Tables 1–4). Only Mn has been found to interact (relatively) weakly with the vacancy, having only non-vanishing binding energy at first nearest neighbour distance: all other elements exhibit fairly strong interaction with the vacancy up to second nearest neighbour distance, particularly Cu [2,14], Si [7,11] and P [7,11–13] (Table 2). On the contrary, only Mn [10,11] and P [5,12,13] appear to form a stable mixed dumbbell: with all other studied elements the mixed dumbbell is unstable [10,11]. This result is not fully compatible with existing resistivity recovery experiments, which were interpreted by the authors in terms of not only stable FeMn mixed dumbbells, but also stable FeCu, FeNi and FeSi mixed dumbbells [39–41]. However, attractive interactions between solutes and SIAs may exist also in configurations where the solute atom is neighbour to an Fe–Fe dumbbell, without forming a mixed dumbbell. Although in these cases the interaction is generally repulsive, it can be positive for Cu and Si atoms, so that dumbbell trapping by Si atoms and, to a

Table 4
Binding energies (eV) corresponding to high symmetry P interstitial configurations, from SIESTA *ab initio* calculations in 128 + 1 and 250 + 1 atom supercells, at both constant volume and constant pressure [12,13].

		Mixed ⟨1 1 0⟩	Mixed ⟨1 1 1⟩	Octa	Tetra
128 + 1 atoms	V = const.	0.92	0.69	0.96	0.82
	P = const.	0.92	0.79	1.00	0.86
250 + 1 atoms	V = const.	0.90	0.67	0.94	0.79
	P = const.	0.90	0.76	0.97	0.82

Table 3
Self-interstitial/solutes (Si, Mn, Ni and Cu) binding energies (eV) obtained with 54 and 128 atom supercells, for the configurations of Fig. 3, from VASP *ab initio* calculations. For the Mn, the antiferro-magnetic (af) or ferro-magnetic (f) states are indicated (data from [11]).

E_b (eV)	Si		Mn		Ni		Cu		P	
Supercell size (atoms)	54	128	54	128	54	128	54	128	54	128
$1nn^{Tens}$_⟨1 1 0⟩	−0.26	−0.23	−0.36 *f*	−0.36 *f*	−0.14	−0.13	0.06	0.07	−0.36	−0.35
$1nn^{Comp}$_⟨1 1 0⟩	0.24	0.27	0.09 *af*	0.10 *af*	−0.06	−0.06	−0.03	−0.01	0.85	0.83
Mixed_⟨1 1 0⟩	−0.05	0.01	0.36 *af*	0.37 *af*	−0.36	−0.36	−0.53	−0.46	0.96	1.02
$\Delta E_{(\langle 1\,1\,1\rangle - \langle 1\,1\,0\rangle)}$ (eV)	0.66	0.52	0.66	0.59	0.78	0.75	0.85	0.73		

lesser extent, Cu atoms is plausible (Table 3 and Fig. 3) and this may explain the resistivity recovery data, too. For more details, see [10,11].

Migration energies of dumbbells in the presence of solute atoms (Cu, Ni, Mn, Si), for all possible combinations of initial and final configurations (illustrated pictorially in Fig. 3) and different migration paths, have been extensively studied with VASP [10,11]. The results, used to parameterise an atomistic kinetic Monte Carlo model [11,42–44], show that the presence of solutes can have a non-negligible effect on the migration of the single SIA in bcc-Fe. However, the only element (aside from P, see below) which is likely to diffuse via mixed dumbbell mechanism is Mn.

Of particular interest are also calculations in which the interaction of the ⟨1 1 1⟩ crowdion with solute atoms is studied as a function of the distance between the two along the ⟨1 1 1⟩ direction. This study shows that Mn, Cr and, to a lesser extent, Ni have a fairly strong attractive interaction with the crowdion, thereby suggesting that Mn (and Ni) in RPV steels may act as traps for SIA clusters formed by parallel crowdions and these, in turn, may be preferential nucleation sites for Mn and Ni precipitation (Fig. 4) [15]. Such a phenomenon may be at the origin of the formation, at high enough doses, of Ni–Mn precipitates in irradiated low-Cu RPV steels, which have been shown to be the consequence of heterogeneous nucleation [13], although they have been also associated with metastable phases whose formation would occur also via homogeneous nucleation, but would require a time of incubation (late blooming phases) [45].

Owing to the particular importance of Cu precipitation in α-Fe via vacancy diffusion mechanism, the interaction of Cu with vacancies in small Cu-vacancy clusters has been studied extensively, including calculations of vacancy energy barriers in the presence of Cu atoms (specifically the barriers required by Le Claire's model for solute diffusion [46]). Results obtained with VASP can be found in [1,2], while a more recent and extended set of results obtained with SIESTA, generally in agreement with the VASP available results, can be found in [14]. These values have been subsequently used to study the diffusion of Cu–V pairs using AKMC techniques [32,47], revealing the fact that Cu atoms are dragged by vacancies, as well as to parameterise AKMC models of Cu precipitation in Fe [14,43].

P is the only substitutional element found to interact (very) strongly with both vacancies and SIAs, with favourable formation of mixed dumbbells, as well as of octahedral interstitial configurations, based on both VASP and SIESTA calculations [5,12,13], as summarised in Tables 2–4. This suggests that, under irradiation, P can be transported via interstitial mechanism and/or trap SIAs. The mixed dumbbell formation has been estimated to correspond to effective migration energy for the mixed dumbbell of 0.19 eV [12,13], in good agreement with resistivity recovery studies [41], although at variance with other experimental estimates of mixed dumbbell migration in electron-irradiated FeP alloys [48]. The octahedral interstitial configuration is found to be particularly favoured if two P atoms are involved and it may thus be responsible [12,13] for enhanced nucleation of SIA loops in the presence of P, as well as for the higher effective migration energy of the mixed dumbbell (0.79 eV) reported in [48]. Additional information concerning P in Fe from *ab initio* and empirical potential calculations can be found in [35].

P is experimentally known to segregate at grain boundaries (GB) under irradiation and this process is believed to be partially responsible for RPV steel embrittlement, by promoting intergranular fracture [49]. Segregation under irradiation can occur as a consequence of purely kinetic effects, e.g. transport of P by point-defects to point-defect sinks, sustained by the continuous production of point-defects and corresponding supersaturation, as well as due to thermodynamic driving forces, that would allow the same phenomenon to occur under thermal ageing, too, in the absence of point-defect supersaturation. *Ab initio* calculations of P binding energies at GB and free surfaces performed with the SIESTA code, summarised in Table 5, suggest that P segregation is thermodynamically driven, so irradiation is not inducing it, but only enhancing it [12,13]. The observed large difference between binding energies at the surface and at GB, in addition, suggests a strong effect of P in reducing the cohesion of GB in bcc-Fe.

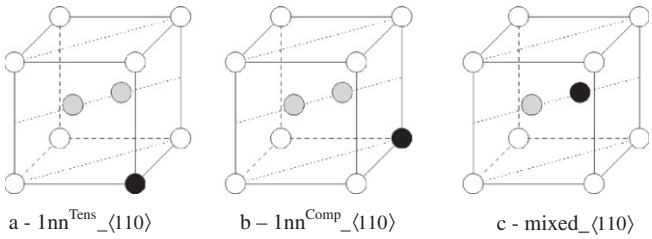

Fig. 3. Schematic representation of the studied configurations involving a dumbbell (grey atoms) and a solute atom (black atom) in bcc-Fe.

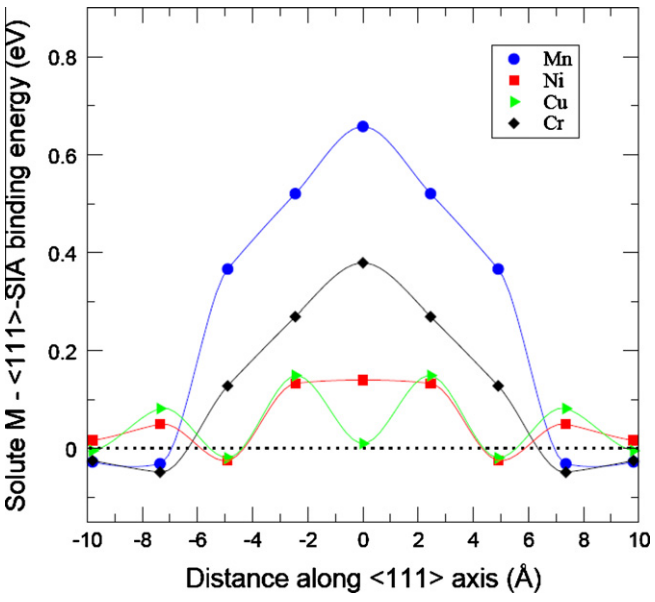

Fig. 4. VASP/PAW calculated binding energy between a solute atom (Mn, Cr, Ni or Cu) and a single crowdion aligned on the same ⟨1 1 1⟩ direction, in Fe, as a function of distance [15].

2.2.2. Interstitial solute atoms (C, N)

The study of C and N atoms in bcc-Fe with VASP [3] provided migration energies (respectively 0.90 and 0.77 eV) and mechanisms (between octahedral sites through tetrahedral sites as

Table 5
P-GB and P-surface binding energies (eV) from SIESTA *ab initio* calculations [21]. First layer indicates either the GB or the surface; 2nd and 3rd layers are the atomic layers right below. "Interstitial site" indicates the case when the P atom is not susbstitutional.

	1st layer	2nd layer	3rd layer	Interstitial site
∑3 {1 1 2} GB	0.00	0.32	0.16	−1.58
∑3 {1 1 1} GB	0.06	1.23	0.54	0.96
Surface 1 1 2	1.59	0.27	–	–
Surface 1 1 1	1.86	1.00	–	–

saddle points) in agreement with experiments. More recent SIESTA calculations confirmed this in the case of C (0.87 eV) [17]. Both C and N are found to have strong attractive interaction with vacancies (without becoming substitutional), N even stronger than C [3], particularly in configurations involving two foreign atoms [3,17]. However, their interaction with single SIAs has been found to be repulsive whenever the C or N atom is located close to the dumbbell [3]. These findings in the case of C have been confirmed by calculations with SIESTA which, in addition, revealed that C atoms, despite their strong attraction to single vacancies, do not stabilise vacancy clusters [21]. It was also established that C atoms have a weak (0.05–0.18 eV), attractive interaction of elastic (i.e. non-chemical) nature with the dumbbell when located at a fairly large distance from it, e.g. in a neighbouring cell, rather than in the same one as the dumbbell [21]. It has also been found that the ⟨1 1 1⟩ crowdion has a weak attractive interaction of elastic nature with C atoms as well [21]: while a single crowdion is unlikely to appear in bcc-Fe, this fact suggests that SIA loops formed by parallel crowdions are likely to be trapped by C atoms (this has been indeed found in studies performed using an empirical potential [50], but the questionable reliability of the used potential calls for confirmation from DFT and/or more reliable potentials). Interactions of similar type and nature, but stronger, exist also in the case of small clusters formed by parallel ⟨1 1 0⟩ dumbbells. Fig. 5 and Table 6 show the configurations of strongest trapping and the corresponding binding energy values.

Table 6
Binding energies (in eV) for the configurations shown in Fig. 5, as calculated with SIESTA [21].

Configuration	E_b
(1) $I_{\langle 1\,1\,0\rangle}$ + C → $I_{\langle 1\,1\,0\rangle}$ C	0.18
(2) $I_{2\langle 1\,1\,0\rangle}$ + C → $I_{2\langle 1\,1\,0\rangle}$ C	0.32
(3) $I_{3\langle 1\,1\,0\rangle}$ + C → $I_{3\langle 1\,1\,0\rangle}$ C	0.41
(4) $I_{\langle 1\,1\,1\rangle}$ + C → $I_{\langle 1\,1\,1\rangle}$ C	0.13

2.3. Point-defect/solute and point-defect/He interactions in austenitic alloys

Ab initio calculations have been performed with VASP in order to characterise the elementary properties of point defects and chemical elements in model fcc alloys. Austenitic FeCrNi systems cannot be easily addressed in a rigorous way by DFT, unless a huge amount of calculations, requiring a very large amount of CPU time, are performed, for different microchemical distributions, so as to derive average effective values. As a starting point, pure fcc Ni has been considered instead, as model "austenitic" (fcc) system, in which the interactions of Fe and Cr atoms, as well as He, between themselves and with point-defects, have been examined.

It is found that the most stable self-interstitial configuration is the ⟨1 0 0⟩ dumbbell, that small clusters of these dumbbells are favourably formed and that, while the mixed Ni–Cr ⟨1 0 0⟩ dumbbell is a favourable configuration, the mixed Ni–Fe ⟨1 0 0⟩ dumbbell is not. Cr–Cr pairs exhibit somewhat attractive interaction, Fe–Fe pairs do not and both elements hardly interact with the vacancy. Nonetheless, the migration energy of a Cr atom is significantly lower than that of Fe, which is in turn significantly lower than that of Ni (0.79 < 0.94 < 1.05 eV) [22].

He in Ni behaves in virtually the same way as in Fe (see e.g. [9] for results in Fe): it prefers being substitutional to interstitial (in the latter case it is stable in a tetrahedral site), many He atoms can be favourably inserted in a vacancy and He_mVac_n clusters are highly stable, the binding energy increasing with the number of vacancies (Fig. 6). Interestingly, while He atoms hardly interact with substitutional solute atoms (Fe, Cr), they have a somewhat attractive interaction with self-interstitials and, in the absence of vacancies, may form favourable He(T) clusters (clusters of He atoms in tetrahedral interstitial position) [22].

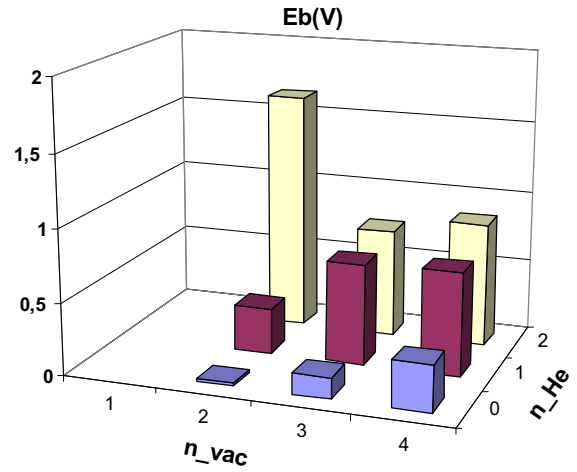

Fig. 6. Binding energy (eV) of a vacancy to small He_mVac_n complexes in Ni (VASP/PAW results) [22].

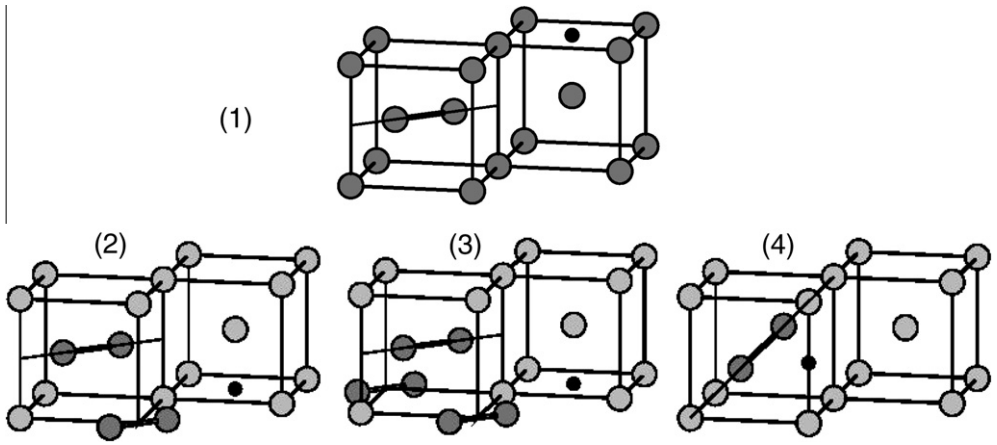

Fig. 5. Pictorial representation of the most attractive configurations of SIA clusters-C atom complexes (corresponding binding energy values are given in Table 6).

3. Development and comparison of advanced potentials for α-Fe

The bcc-Fe potential by Mendelev et al. [34], developed little before the start of the Project, and its slightly more recent version, developed within the Project [35], represent, in the framework of an embedded atom method (EAM) approach [51], a clear advance compared to previously available potentials for this metal, using *ab initio* results as a reference. This is clearly demonstrated in the comparison between bcc-Fe potentials reported in [36]. As such, this type of potentials, in either of its two very similar versions (potential nr. 2 from [34], henceforth denoted as M03, and Fe–Fe potential from [35], henceforth A04), have been widely employed within the Project for molecular dynamics simulations and have been used as Fe–Fe part for the construction of all the alloy potentials (see Section 4). Nonetheless, on the one hand, since the beginning it was clear that there was still room for improvement of these "Mendelev-type" potentials; on the other, a formalism capable of including in the picture also magnetism (the fundamental characteristic of bcc-Fe) was needed. Two parallel approaches were therefore pursued within the Project: (i) development of an advanced many-body potential formalism including the description of magnetism, finally produced through a combination of the Stoner and the Ginzburg–Landau models [52,53]; and (ii) development of an advanced EAM potential, based on the Mendelev approach, tailored in such a way that point-defects and their clusters are better described, by working on the fitting procedure (work still ongoing; some results obtained with a potential produced within such a framework are reported in [36]).

3.1. Development of a 'magnetic' potential for bcc-Fe

Prior to the Project a formalism for a magnetic potential in iron, based on extending Finnis–Sinclair to two bands with an additional term favouring maximum spin, was proposed [54]. The theory of this was developed further during the Project [55]. In parallel, an empirical many-body potential formalism that introduces an explicit magnetic contribution to the energy of interaction between atoms in α-Fe has been developed within the Project [52]. The approach is based on a combination of the Stoner and the Ginzburg–Landau models [56,57], after finding that the symmetry broken solutions describing the spontaneous magnetisation of atoms are responsible for the link between magnetism and interatomic forces. A phenomenological embedding function of the many-body, *multi-branching* interatomic potential has been therefore derived from the exact solution of the Stoner model found in [52], simplified in the Ginzburg–Landau approximation. This embedding function has the form

$$F[\rho] = -A\rho^{1/2} - (B/\ln 2)(1 - (\rho/\rho c)^{1/2})\ln(2 - \rho/\rho c)\Theta(\rho c - \rho) \quad (1)$$

Here, ρ_c is a critical value of the effective electron density and $\Theta(x)$ is the Heavyside step function (1 for $x > 0$, 0 elsewhere). In this expression the first term coincides with the Finnis–Sinclair form for the embedding function, stemming from the second moment tight-binding approximation, while the second term, switched on only when $\rho < \rho_c$ and $B \neq 0$, embodies the magnetic contribution to the energy associated with symmetry breaking. This function is continuous with its first derivative at $\rho = \rho_c$, but presents a cusp discontinuity at that point, corresponding to the onset of a symmetry broken magnetic solution, similar to the one describing a second order phase transition.

By adjusting the effective pairwise density functions and pairwise interactions, the energy of interatomic interactions is cast in a form that describes either the equation of state for the non-magnetic and magnetic configurations (case study I), or the energies of vacancy and self-interstitial point defects in α-Fe (case study II). Obtaining correct descriptions for both features at the same time proved unfeasible. Overall, the model provides a valuable means to assign a magnetic energy contribution to the cohesive energy and defect formation energies (for example by allowing the association of a magnetic moment to atoms and defects), as well as a framework to describe the relative stability of the bcc versus fcc phases in Fe at 0 K. More details can be found in [52,53].

The "case study II" version of this type of potential (denoted as D05), fitted to describe correctly the relative stability of single self-interstitial configurations in bcc-Fe as known from DFT calculations, has been used within the Project for a thorough comparison with Mendelev-type potentials and DFT. The results are reported in [36]. It is found that this potential performs clearly much better than earlier ones for bcc-Fe, represented in the comparison exercise by the well-known and widely used bcc-Fe potential from [58] (denoted as A97). However, in general Mendelev-type potentials perform somewhat better, as compared to the available DFT reference values, both qualitatively and quantitatively. In particular, while self-interstitial type defects are described with D05 as well as with any Mendelev-type potential, with only subtle and minor differences, vacancy type defects are assigned a somewhat too high binding energy by D05 and their migration energy is also too high with this potential. In addition, D05 has a problem with the thermal expansion and the predicted screw dislocation core exhibits threefold symmetry (the same as with A97), instead of being compact as in DFT. These and other shortcomings are, however, likely to be removable after more careful fitting, within the same formalism, and work in this sense has been recently performed [59].

3.2. Improved Mendelev-type potential

The M03 potential was carefully fitted to properties of liquid iron and *ab initio* values for the $\langle 1\,1\,0\rangle$ and $\langle 1\,1\,1\rangle$ dumbbell formation energies. It is capable of reproducing correctly the relative stability of these two possible SIA configurations, thereby representing an improvement over earlier ones (e.g. [58]). In addition, its use has revealed that it predicts correctly, at least qualitatively, a whole lot of features in agreement with DFT [36]. Its more recent version, A04, removes a small problem of thermal expansion, by slightly modifying the embedding function, and its performance is generally comparable with that of M03, or even somewhat better in a few cases [36]. Nonetheless, a number of weaknesses remain, revealed as the number of available DFT data concerning defects in Fe increases. In particular, although the discovery of the stability of non-parallel SIA cluster configurations (Fig. 1) [16] was made using Mendelev-type potentials, the comparison of the description that these potentials give for these configurations with the DFT description further revealed their inadequacy in many cases. It is believed that more accurate potentials can be produced within the same formalism, by working on the fitting strategy. One of the objectives of the Project was therefore to develop a new potential, based on the same approach as Mendelev's, where as many present weaknesses of M03 and A04 as possible are removed.

A first version of a new Mendelev-type potential (developed at CEA Saclay and denoted here as M07), fitted to a large set of defect energies from SIESTA calculations, is proposed in [36], where it is compared with the other Mendelev-type potentials, as well as with D05 and A97. This released version exhibits closer agreement to reference *ab initio* data for SIA formation and migration energies, as compared to M03 and A04, although overall the performance is similar. This potential has been used to test a number of defect properties, for example the behaviour at finite temperature of small SIA clusters and the relative stability of $\langle 1\,1\,1\rangle$ versus $\langle 1\,0\,0\rangle$ loops. By calculating the formation entropy of small clusters, it

was found that, although the ⟨1 1 0⟩ configuration is the most stable at 0 K, tri- and quadri-interstitial become more stable in the ⟨1 1 1⟩ configuration above, respectively, 700 and 300 K, in this agreeing qualitatively with predictions made using the A04 potential [60]. Even more stable at high temperature are, in general, the NPC, as is briefly described in the next section.

3.3. Non-parallel SIA cluster configurations and ⟨1 0 0⟩ versus ⟨1 1 1⟩ loops

As anticipated in Section 2.1, the discovery of the stability of the non-parallel SIA cluster configurations shown in Fig. 1 has challenged the accepted picture of (i) slowly migrating small SIA clusters in ⟨1 1 0⟩ configurations and (ii) one-dimensionally gliding SIA clusters in ⟨1 1 1⟩ configurations, as the only two possibilities to be considered in microstructure evolution models. These NPCs cannot migrate as such and need first to unfault to parallel-dumbbell configurations in order to do so (self-trapping configurations). Depending on their relative stability, which is temperature-dependent [16], the impact on the effective mobility of SIA clusters, and therefore on the microstructure evolution of irradiated bcc-Fe alloys, will change. Since different calculation methods give different indications concerning NPC stability, it is impossible to be fully quantitative. However, qualitatively the message is clear: the existence of NPCs implies that SIA clusters can be, depending on the situation, both mobile and immobile and this fact may explain why, up to now, some experimental results (e.g. resistivity recovery stages) could be interpreted by postulating SIA cluster immobility [8], while other results require, to be reproduced, that SIA clusters should be highly mobile, although with traps [61].

Another open issue on which the NPC may have a role concerns the formation of ⟨1 0 0⟩ versus 1/2⟨1 1 1⟩ loops. Both loops are experimentally long known to form [62], but according to isotropic elasticity theory the former loops are less stable than the latter. When using interatomic potentials, the relative stability is unclear, as each potential predicts a different behaviour [36,63]. In addition, there is no consensus concerning the mechanism whereby ⟨1 0 0⟩ loops are nucleated or formed, e.g. as a consequence of a reaction between 1/2⟨1 1 1⟩ loops or by spontaneous transformation from the latter type to the former [64–66]. Recent work, based on anisotropic elasticity theory, suggests that, as a consequence of the magnetic transition undergone by iron, ⟨1 0 0⟩ loops become stable at high temperature [67]. Such a feature is consistent with the behaviour of NPC. In addition, it is possible to show that NPCs can grow into clusters having an effective ⟨1 0 0⟩ orientation [16,66]: ⟨1 0 0⟩ loops may therefore be nucleated as NPC.

4. Development and comparison of advanced potentials for Fe alloys

Even supposing that fully reliable interatomic potentials for pure elements, especially Fe, were available, the fitting of potentials for alloys poses a series of problems, unknown in the case of pure elements, which need to be specifically addressed. First and foremost, a potential for an alloy should prove to be reasonably consistent with the corresponding phase diagram. In addition, in the specific case of the study of radiation damage, it becomes extremely important to reproduce as correctly as possible the interaction energies between point-defects and solute atoms (so definable in the limit of diluted alloys), including their effect on the migration properties. Work in this direction has been carried out within the Project, on two fronts: (i) development of potentials for substitutional alloys, namely FeCu, FeNi and the ternary FeCuNi system, where consistency with thermodynamics was the main goal; and (ii) development of potentials for interstitial alloys, namely FeC, with emphasis on the proper prediction of the interaction of the interstitial alloying species and point-defects.

In all cases, the Fe–Fe part was chosen to be a Mendelev-type potential (either M03 or A04). The far-sightedness of this early choice is proven by the exercise of comparison between Fe potentials reported in [36]. For the considered substitutional elements (Cu, Ni) the most recent potentials available from the literature [68,69] were used whenever possible (in the case of Ni, an older potential by Voter and Chen [70] turned out to provide, eventually, better results for the alloy). The carbon–carbon interaction represents an exception, because no fully satisfactory carbon–carbon potential compatible with an EAM type potential, such as M03 and A04, was available from outside the Project and its development, together with the development of a satisfactory FeC potential, represented a major challenge to be addressed. It should be noted that producing advanced potentials for alloys required first of all the development of advanced codes and procedures to fit them and this task represented a large part of the work done on Fe alloy potentials within the Project.

4.1. Potentials for substitutional alloys

4.1.1. FeCu potential consistent with the experimental phase diagram

Prior to the start of the Project, two FeCu potentials existed and had been widely used for the study of radiation damage production, evolution and interaction with dislocations by means of atomistic simulation tools, denoted here as AB97 [58] and LF98 [71]. Neither was, however, fully satisfactory: the former failed to reproduce the correct solubility limit of Cu in Fe, being off by an order of magnitude [72], while the latter, among other problems, was based on an Fe–Fe potential [73] that did not reproduce the ⟨1 1 0⟩ dumbbell as the most stable SIA configuration.

A new FeCu interatomic potential (CO5.20) was thus developed within the Project [74], using, for the pure elements, the M03 potential for α-Fe and, for Cu, the potential from [69]. The fitting of the cross part was performed by applying a novel procedure, based on the idea of using phase diagram points as reference fitting data [75]. This was made possible by defining the alloy configurations, with which a certain enthalpy is associated, by means of on-site spin functions, then averaged using the correlation function formalism, and by adopting the cluster variation method (CVM) approximation to provide an expression for the entropy [76–78]. This methodology was implemented in a code baptised FITMIX [79]. The traditional EAM [51] was then used to express the energy of the system, in such a way that the free energy becomes a func-

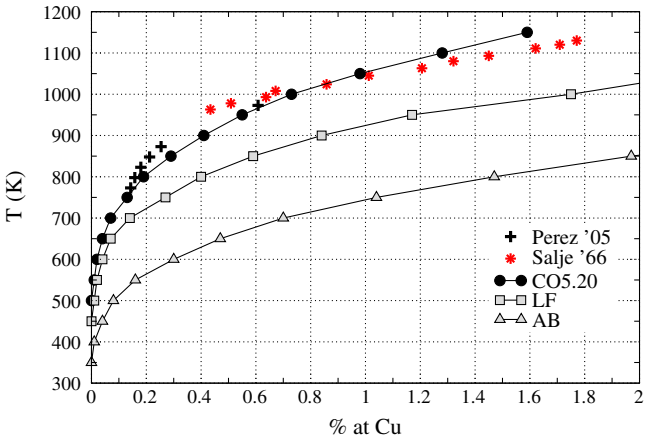

Fig. 7. Solubility limit according to three interatomic potentials, namely CO5.20 [74], LF98 [71] and AB97 [58], as compared to experimental data from Salje and Feller-kniepmeier [80] and from Perez et al. [81].

tion of the parameters of the potential. In this way, a potential providing a solubility limit for Cu in Fe (and Fe in Cu) in close agreement with experimental measurements was produced (Fig. 7). In addition, the potential was fitted to CuCu and Cu-vacancy binding energies consistent with *ab initio* indications [2]. Control was also exerted on the vacancy migration energy barriers in the presence of a Cu atom, so as to approach the *ab initio* values and to provide a vacancy dragging effect (motion of the Cu-vacancy pair as a whole), suggested by both experimental [82] and theoretical studies [47] and hitherto not reproduced by any FeCu potential. Finally, attention was paid to have an acceptable description of the interaction between a self-interstitial atom and a Cu atom, also based on *ab initio* indications [1]. It is believed that, in the framework of the EAM approach, the CO5.20 potential is currently the best available for the description of radiation effects in FeCu alloys. For more details see [74,75].

4.1.2. An FeNi potential for the simulation of austenitic alloys

In the absence of a ternary FeCrNi potential, and seen the difficulty of producing one, a first FeNi potential was developed, aimed at modelling the 316 austenitic steel used in the nuclear industry, with the main purpose of simulating with it displacement cascades by MD. This was done after having discarded, following careful evaluation, the potentials for FeNi available from the literature. State-of-the-art EAM potentials were adopted for the pure elements, taken from [35] and [68] for, respectively, α-Fe and Ni. The fitting approach for the cross term was based on the use of *ab initio* configurations produced with VASP. The potential was built starting from twelve *ab initio* configurations and the elastic constants of the $FeNi_3$ compound: the bcc–fcc transition with this potential occurs, for random alloys, in the correct composition range, i.e. around 25% Ni (Fig. 8), but the equilibrium lattice parameter is slightly overestimated and the C_{11} elastic constant is not well reproduced. However, attempts at reproducing the correct lattice parameter and improving the elastic constants led the random fcc phase to become favoured over the random bcc alloy only above 55% Ni. Thus, the former potential was kept and stiffened for the simulation of displacement cascades. The diffusivity of the single self-interstitial atom in the fcc $Fe_{55}Ni_{45}$ alloy and in pure Ni was also studied, finding that the addition of Fe slows down the interstitial, in qualitative agreement with experimental observations [83].

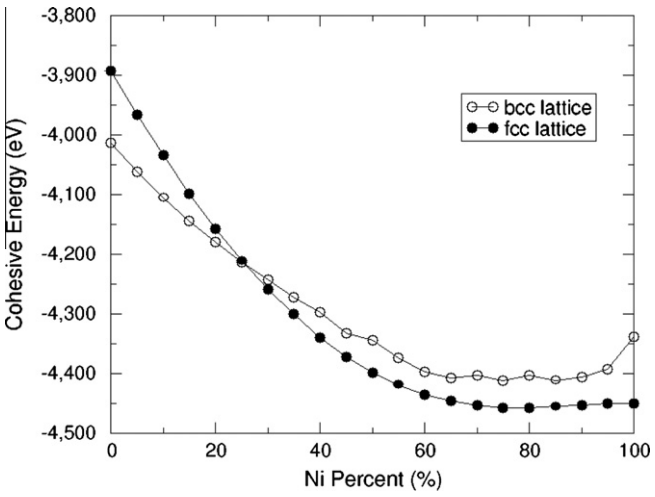

Fig. 8. Relative stability of the bcc and fcc phases (random solutions at 0 K) according to the FeNi-JMR potential.

This potential, from now on denoted as FeNi-JMR, was later more carefully analysed from the thermodynamic standpoint, by building the phase diagram that it embodies and by calculating the energy that it predicts for a large number of ordered structures. It was found that, despite favouring in an apparently correct way the fcc versus the bcc phase (Fig. 8), it predicts as ground states at low temperature a large number of ordered structures, most of which do not exist in reality. While this fact is not expected to be a major problem for high temperature cascade simulations by MD, it is desirable, on general grounds, to have a better reproduction of the thermodynamic properties of the FeNi system. In addition, in connection with RPV steel applications, it is also important to have a potential reproducing as correctly as possible the point-defect/solute interaction in ferritic FeNi alloys. These considerations prompted further work, aimed at applying a fitting approach based on the correlation functions, as for the FeCu system, for the development of another FeNi potential.

4.1.3. A thermodynamically improved FeNi potential

The FeNi system exhibits ordered intermetallic phases, which are key issues to be tackled when creating an FeNi potential consistent with thermodynamics. From experimental evidence $L1_2$ $FeNi_3$ is accepted to be a stable phase, while Fe_3Ni ($L1_2$) and FeNi ($L1_0$) are assumed to be metastable phases, although some sources [84–86] suggest $L1_0$ FeNi to be included as a stable phase in the phase diagram. In addition, at high temperature there is a region of complete solid solubility in the fcc phase. A potential should therefore, at least, obtain the correct 0 K ground states and avoid possible unwanted ones, while reproducing a large region of miscibility in the fcc phase at finite temperature. In order to have a control over 0 K ground states, the possible ones are determined using a rigid lattice Ising model and the theory of correlation function space (the relevant methodology is implemented in the FITMIX code [79]). Using this theory and a compromise between the maximum unit cell size for a possible ground state, as well as the number of ground states to be addressed, 99 ordered structures were retained for the bcc phase and 87 for the fcc phase (from now on referred to as the BCC-99 and FCC-87 ordered structures – see [75] for more details). In addition, since the proposed FeNi potential is to be used for the development of the ternary FeNiCu potential (see next section), of interest mainly as ferritic model alloy for RPV steels, special attention was devoted, upon fitting, to reproduce at best the solute/point-defect interaction in bcc-Fe.

The strategy therefore consisted of fitting to (i) thermodynamics and (ii) defect energies in the bcc-Fe matrix. To obtain the correct thermodynamic behaviour, the mixing enthalpy curve (of importance at high temperature) was fitted and the correct ground states (of importance at low temperature) were kept under control. At the same time, care was taken to keep acceptable values for the migration barriers (via vacancy mechanism), as well as for the Ni–Ni and Ni-vacancy binding energies. After this first fitting stage, extra nodes were added in the 2.5–2.1 Å range, to fit to the binding energy of dumbbell configurations. Fig. 9 shows the comparison between the structure energies with the FeNi-JMR potentials and the new FeNi potential (FeNi-071115-2), based on M03 for Fe [34] and on the Ni potential from [70]. While FeNi-JMR does not stabilise the correct ground states, FeNi-071115-2 does. Table 7 compares the performance of both potentials concerning point-defect/solute interaction in bcc-Fe, showing that the FeNi-071115-2 potential provides indeed reasonable fitting to reference *ab initio* data, particularly allowing for the discrepancy that exists also between different DFT methods (USPP and PAW). The potential proved also reasonable, as compared to *ab initio* data, in describing point-defect/solute interaction in the Ni-rich fcc phase. For more details, see [87].

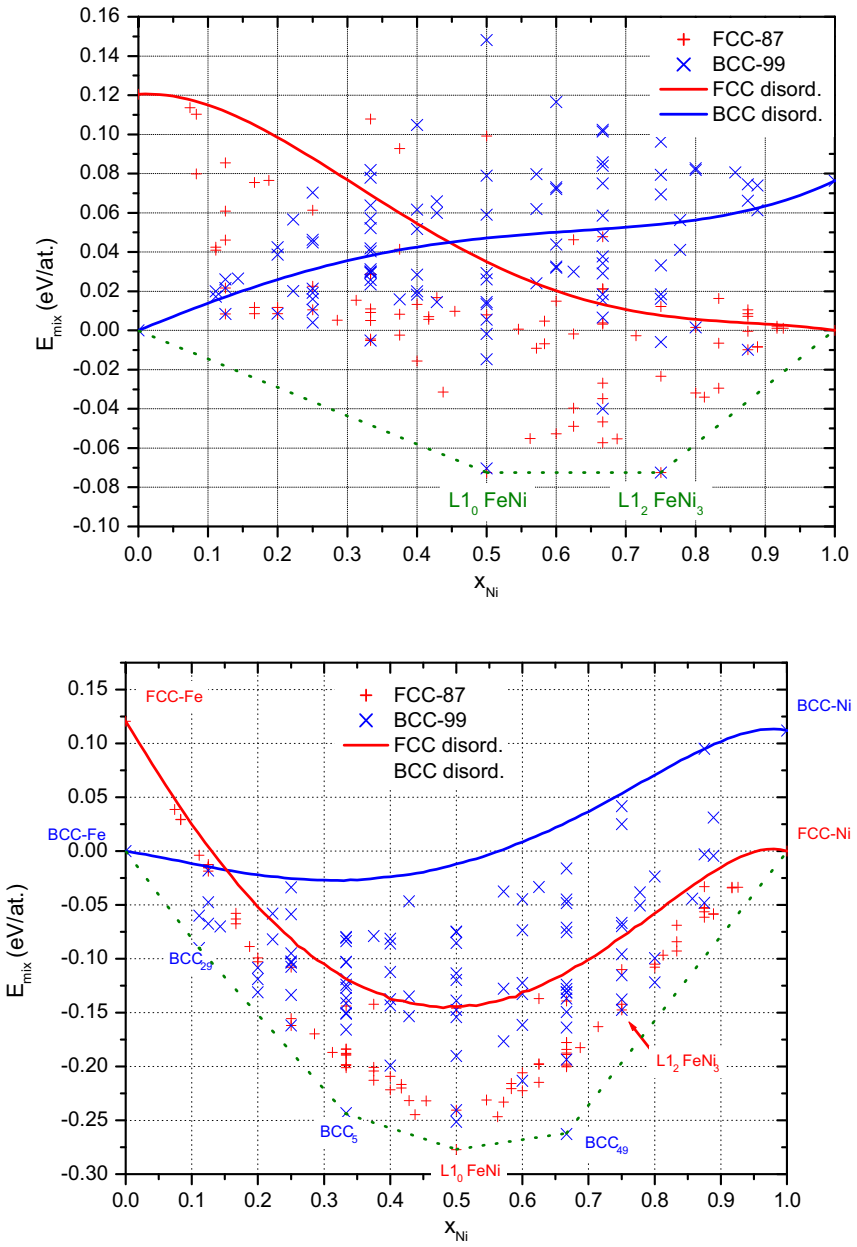

Fig. 9. Mixing energies for the BCC-99, FCC-87 structures and the BCC and FCC disordered phases calculated with the FeNi-071115-2 (above) and the FeNi-JMR (below) potentials.

4.1.4. A ternary FeCuNi potential

Using as a basis the FeNi-071115-2 potential, and the FeCu potential produced earlier (CO5.20) with the same emphasis on thermodynamics and bcc defect configurations, the CuNi cross potential was developed to describe the ternary FeCuNi alloy. Using FITMIX and the same methodology as in the FeNi case, the CuNi cross potential was fitted to the mixing enthalpy curve and to ternary CuNi complexes data in the bcc-Fe matrix, as known from *ab initio* calculations. Fair agreement was found between the experimental CuNi phase diagram and the phase diagram built from the CuNi potential [88]. In addition, as shown in Table 8, reasonable agreement is obtained between the few available *ab initio* data for CuNi complexes, including point-defects (mixed dumbbell) in bcc-Fe, and those produced with the potential. Further fine-tuning will be possible *a priori*, as soon as more reference *ab initio* "FeCuNi" data become available.

4.2. FeC potentials

A proper description of C in Fe is the first fundamental step to approach systems that can be defined as steels. However, the task of fitting a potential for FeC represents a challenge. C is an interstitial element in bcc-Fe (the substitutional position is unfavourable [3]) and a potential must correctly allow for the fact that the preferred interstitial position is octahedral and is significantly more stable than the tetrahedral one, which may represent the saddle point for migration [3]. In addition, C atoms do not cluster, but are strongly bound to close-by vacancies, while they are weakly repulsive to close-by self-interstitials (aside from the attractive long-range interaction of probable elastic origin described in Section 2.2.2) [3]. Finally, in the presence of a vacancy two close-by C atoms exhibit a strong attraction of covalent origin [3]. Including all these features in an EAM-like potential is not straightforward,

Table 7
Solute–solute and point-defect/solute binding energies (eV) according to potentials and DFT calculations (128 atom supercells, with VASP) (For the dumbbell/solute configurations, see Fig. 3).

	FeNi-071115-2	FeNi-JMR	128 atom USPP [11]	128 atom PAW [98]
E_{sub} Ni	0.10	−0.74	−0.17	0.13
E_b Ni–Ni (1nn)	−0.02	−0.19	−0.10	0.02
E_b Ni–Ni (2nn)	0.11	−0.15	−0.02	0.00
E_b V–Ni (1nn)	−0.02	0.04	0.03	0.12
E_b V–Ni (2nn)	0.10	−0.09	0.17	0.20
E_b ⟨1 1 0⟩ Fe–Ni	−0.36	−1.81	−0.36	−0.16
E_b ⟨1 1 0⟩ Fe–Fe, Ni $1nn^{Tens.}$	−0.15	0.07	−0.13	0.02
E_b ⟨1 1 0⟩ FeFe, Ni $1nn^{Comp.}$	−0.13	−0.91	−0.06	0.05
E_b ⟨1 1 0⟩ Fe–Ni, Ni $1nn^{Comp.}$	−0.36	−0.19	−0.32	
E_b ⟨1 1 0⟩ Ni–Ni	−0.58	−2.67	−0.30	
E_b ⟨1 1 1⟩ Fe–Ni	−0.03	−0.07		
E_b ⟨1 1 1⟩ Ni–Ni	−0.06	−0.33		

Table 8
Binding energies (eV) of CuNi complexes in the bcc-Fe matrix (DFT data from [11]).

	FeNiCu-071115-2	128 atom VASP/USPP
E_b Cu–Ni (1nn)	0.01	0.02
E_b Cu–Ni (2nn)	0.07	−0.01
E_b ⟨1 1 0⟩ Cu–Ni	−0.37	−0.50

everything cannot be correctly grasped and the only possible strategy for fitting a potential involves the extensive and clever use of the available *ab initio* data.

A first attempt to fit an FeC potential was made at the beginning of the Project. In that case it was observed that a pairwise potential was not sufficient to reproduce all *ab initio* configurations and an embedding part was introduced. For the carbon–carbon interaction, with all its limitations, the pair potential by Ruda et al. [89] was used. Three FeC potentials were fabricated in this way, based on different Fe–Fe potentials, namely potential B from [73], potential A97 [58], and the Mendelev-type potential A04 [35]. The three of them performed in a broadly similar way when contrasted to the *ab initio* database of configurations and energies in FeC and better than the early Johnson potential [90]. Using these potentials, a study of C-loop interactions was started, finding a positive binding energy (~0.4-0.5 eV) for some configurations. The FeC potential built using A04 [35] (from now on denoted as FeC-RAU) has then been successfully used to study the diffusion coefficient of C in bcc-Fe, the interaction of C atoms with a screw dislocation and the lattice parameter evolution versus C content (tetragonal lattice structure), finding results consistent with experiments [91]. Preliminary data for the modelling of the Snoek peak in internal friction experiments have also been produced [91]. However, weak points remained. In particular, the carbon–carbon interaction, as described by the potential taken from the literature [89], was not fully satisfactory and could not reproduce the covalent bond strength revealed by DFT calculations when two C atoms are close to a vacancy [3]. In addition the C atom/dumbbell interaction kept being attractive for configurations for which it is repulsive according to *ab initio* evidence [3].

A second attempt was therefore made, using another advanced fitting code, developed within the Project, which allows both specified energy differences between sets of *ab initio* configurations and relevant forces to be fitted [92]. Options also exist to relax particle coordinates in the fitting procedure and to include stress contributions in the objective function being optimised. The fitting itself is performed using a combination of a global optimiser (genetic algorithm or direct search technique) and a local gradient-based Levenberg–Marquardt algorithm [93].

A series of EAM-compatible FeC potentials, all based on the FeFe A04 potential [35], has thereby been produced. The key point to produce a qualitative improvement compared to all other potentials and, in particular, the early Johnson potential [90], was the introduction of a fully saturated covalent bonding between the C atom and its first two Fe neighbours in the octahedral site, instead of stabilising the latter configuration by binding the C atoms to the six first *and* second nearest neighbours, as by doing so it is unavoidable that the C atom binds close-by dumbbells, too. The use of this EAM-compatible saturating potential form allows also the CC covalent bonding at vacancies to be correctly treated. The best-fit FeC potential of this type is described in [92]. A thorough comparison between the FeC-RAU, other potentials from the literature (both early ones, such as [90], and recent ones, such as [94], which has any way the shortcoming of being based on an old Fe potential) and the present potential shows that the latter describes as well as the others the distortion around the C atom in a bcc-Fe lattice, its migration energy and the interaction with a second C atom. The attraction to the vacancy and, more importantly, the repulsion from a close-by dumbbell (with weak attraction at a distance from it) are also well reproduced and this potential is the only one that succeeds in reproducing both at the same time. Also the strength of the CC covalent bond in the presence of a vacancy is properly reproduced.

5. Concluding remarks

A large set of DFT data have been produced on configuration energies of point-defects and their clusters, as well as migration energies in pure α-Fe, including the effect of solute–defect interaction, both for substitutional (Cu, Ni, Mn, Si, P) and interstitial (C, N) solute atoms, has been produced. Data of relevance for austenitic alloys are still limited in number, but some of them exist and more are being produced. These data have greatly enhanced our level of understanding of microstructural processes occurring under irradiation in model alloys and steels used in existing nuclear power plants, as this overview has tried to highlight. The work that the DFT community should mainly face, now, is that of mutual validation of results. Generally VASP (USPP and PAW) and SIESTA data are broadly consistent and when this happens the data themselves become more trustworthy. However, the choice of different DFT approaches may produce *quantitatively* different results and it is important to establish the range of variability when these differences appear, particularly when also *qualitative* differences arise. The case in which this discrepancy is most worrying and important at the same time is that of the non-parallel SIA cluster configurations.

The knowledge acquired from DFT studies is being transferred, using one approach or another, to empirical interatomic potentials and is also being directly used to fit kinetic Monte Carlo models [43]. The EAM-like advanced potentials for pure Fe can be divided in two classes: Mendelev-type and 'magnetic'. At the moment, although both represent a clear improvement compared to earlier potentials, the former class is found to perform somewhat better than the second one, when compared to *ab initio* data. The reason for the difference is likely to be ascribable purely to the care put in the fitting. In itself, the formalism of the 'magnetic' potential, by including explicitly an assessment of the magnetic contribution to the total energy, is interesting and promising. However, more work on its parameterisation is needed. Along this line, two re-parameterisations of the 'magnetic' potentials have been recently published [59] and they need now to be thoroughly tested within the involved community. The Mendelev-type potentials already

Table 9
Available empirical potentials from within (published and yet unpublished) and without (published) the Project.

Fe	M03 [34], A04 [35] and further improvements (e.g. M07 [36]), D05 [52,53] and further improvements (e.g. [59,93]), bond-order [95]
FeCu	CO5.20 [74]
FeNi	FeNi-JMR, FeNi-071115-2 [87]
FeNiCu	[88]
FeP	[35]
FeCr	2BM [96], CDM [97]
FeC	FeC-RAU [91], FeC [92]
FeHe	[98,99]

allow, to some extent, DFT studies to be 'extrapolated' to ranges inaccessible to DFT. However, on many instances differences exist between potentials of this same class (see [36]) and, whenever a clear *ab initio* or experimental reference is lacking, the results must be taken with care and considered as possibilities, rather than certainties.

On the Fe alloy potential side, within the framework of reliability of Mendelev-type potentials for Fe, advances have been also made and these were determined not only by the systematic use of *ab initio* data for the fitting, but also by the attention paid to a correct reproduction of the thermodynamic properties of the alloys, especially in the case of substitutional alloys, such as FeCu and FeNi. The problem of FeC, as expected, was a particularly tough one, especially if the existence of covalent carbon–carbon bonding has to be allowed for. Nonetheless, two FeC potentials based on state-of-the-art Fe potentials are at least available for studies concerning the interaction of point-defect clusters and dislocations with a single C atom, one of them being able to reproduce correctly most *ab initio* configuration energies, including the interaction between a C atom and close-by dumbbells.

The available potentials do not cover, yet, the full range of elements that appear in RPV steels. However, an FeCuNi ternary potential – the first carefully designed and taylored for radiation damage studies, to our knowledge – is now available and complex substitutional element effects can be hence studied at the atomic level, at the time-scale accessible to molecular dynamics, as well as, separately, the effects of the presence of C. In the case of austenitic steels, FeNi is the best model alloy immediately available, but the possibility of fabricating a ternary potential for an FeNiCr ternary alloy may be now at reach.

In a broader perspective, i.e. including work done outside the Project and looking forward to a continuation of the work performed in it in future Projects, the landscape is encouraging. Table 9 summarises the advanced empirical potentials for alloys currently available and based on state-of-the-art Fe potentials that we have knowledge of, from within *and without* the Project. It is easy to see that future Projects, for both internals and RPV steels, may take seriously the possibility of developing potentials for multicomponent systems.

References

[1] C. Domain, C.S. Becquart, Phys. Rev. B 65 (2001) 024103.
[2] C.S. Becquart, C. Domain, Nucl. Instrum. Methods Phys. Res. B 202 (2003) 44–50.
[3] C. Domain, C.S. Becquart, J. Foct, Phys. Rev. B 69 (2004) 144112.
[4] C.-C. Fu, F. Willaime, P. Ordejón, Phys. Rev. Lett. 92 (17) (2004) 175503.
[5] C. Domain, C.S. Becquart, Phys. Rev. B 71 (2005) 214109.
[6] F. Willaime, C.C. Fu, M.C. Marinica, J. Dalla Torre, Nucl. Instrum. Methods B 192 (2005) 228.
[7] E. Vincent, C.S. Becquart, C. Domain, Nucl. Instrum. Methods Phys. Res. B 228 (2005) 137.
[8] C.-C. Fu, J. Dalla Torre, F. Willaime, J.-L. Bocquet, A. Barbu, Nature Mater. 4 (2005) 68.
[9] C.-C. Fu, F. Willaime, Phys. Rev. B 72 (2005) 064117.
[10] E. Vincent, C.S. Becquart, C. Domain, J. Nucl. Mater. 359 (2006) 227.
[11] E. Vincent, PhD Dissertation, University of Lille I, 2006.
[12] E. Meslin, C.-C. Fu, A. Barbu, F. Gao, F. Willaime, Phys. Rev. B 75 (2007) 094303.
[13] E. Meslin, PhD Dissertation, University of Rouen, 2007.
[14] F. Soisson, C.-C. Fu, Sol. State Phenom. 129 (2007) 31; F. Soisson, C.-C. Fu, Phys. Rev. B 76 (2007) 214102.
[15] P. Olsson, E. Vincent, C. Domain, Proc. AES-ATEMA (2007) 405.
[16] D. Terentyev, T.P.C. Klaver, P. Olsson, M.-C. Marinica, F. Willaime, C. Domain, L. Malerba, Phys. Rev. Lett. 100 (2008) 145503.
[17] C.-C. Fu, E. Meslin, A. Barbu, F. Willaime, V. Oison, Solid State Phenom. 139 (2008) 157.
[18] J.M. Soler, E. Artacho, J.D. Gale, A. Garcia, J. Junquera, P. Ordejon, D. Sanchez-Portal, J. Phys. Condens. Matter. 14 (2002) 2745.
[19] G. Kresse, J. Hafner, Phys. Rev. B 47 (1993) 558; G. Kresse, J. Hafner, Phys. Rev. B 49 (1994) 14251.
[20] G. Kresse, J. Furthmüller, Comput. Mater. Sci. 6 (1996) 15.
[21] C.-C. Fu, Reported to Perfect, unpublished.
[22] C. Domain, C.S. Becquart, Reported to Perfect, unpublished.
[23] J.P. Perdew, K. Burke, M. Ernzerhof, Phys. Rev. Lett. 77 (1996) 3865.
[24] J.P. Perdew, J.A. Chevary, S.H. Vosko, K.A. Jackson, M.R. Pederson, C. Fiolhais, Phys. Rev. B 46 (1992) 6671.
[25] D. Vanderbilt, Phys. Rev. B 41 (1990) 7892.
[26] P.E. Blöchl, Phys. Rev. B 50 (1994) 17953.
[27] S.H. Vosko, L. Wilk, M. Nusair, J. Can. Phys. 58 (1980) 1200.
[28] F. Gao, D.J. Bacon, Yu.N. Osetsky, P.E.J. Flewitt, T.A. Lewis, J. Nucl. Mater. 276 (2000) 213.
[29] R.A. Johnson, Phys. Rev. 134 (1964) A1329.
[30] N. Soneda, T. Díaz de la Rubia, Philos. Mag. A 81 (2001) 331.
[31] P. Ehrhart, K.H. Robrock, H.R. Schober, in: R.A. Johnson, A.N. Orlov (Eds.), Physics of Radiation Effects in Crystals, Elsevier, Amsterdam, 1986, p. 7 (and references therein).
[32] F. Djurabekova, L. Malerba, C. Domain, C.S. Becquart, Nucl. Instrum. Methods Phys. Res. B 255 (2007) 47.
[33] F. Djurabekova, L. Malerba, R.C. Pasianot, P. Olsson, K. Nordlund, Philos. Mag. Lett. 90 (2010) 2585.
[34] M.I. Mendelev, S. Han, D.J. Srolovitz, G.J. Ackland, D.Y. Sun, M. Asta, Philos. Mag. 83 (2003) 3977.
[35] G.J. Ackland, M.I. Mendelev, D.J. Srolovitz, S. Han, A.V. Barashev, J. Phys. Condens. Matter 16 (2004) S2629.
[36] L. Malerba, M.C. Marinica, N. Anento, C. Björkas, H. Nguyen, C. Domain, F. Djurabekova, P. Olsson, K. Nordlund, A. Serra, D. Terentyev, F. Willaime, C.S. Becquart, Comparison of empirical interatomic potentials for iron applied to radiation damage studies 406 (2010) 19.
[37] A. Möslang, E. Albert, E. Recknagel, A. Weidinger, Hyperfine Interact. 15/16 (1983) 409.
[38] G. Brauer, K. Popp, Phys. Status Solidi B 102 (1987) 79.
[39] F. Maury, A. Lucasson, P. Lucasson, Y. Loreaux, P. Moser, J. Phys. F: Met. Phys. 16 (1986) 523.
[40] F. Maury, A. Lucasson, P. Lucasson, P. Moser, F. Faudot, J. Phys.: Condens. Matter 2 (1990) 9291.
[41] H. Abe, E. Kuramoto, J. Nucl. Mater. 271 and 272 (1999) 209.
[42] E. Vincent, C.S. Becquart, C. Domain, J. Nucl. Mater. 351 (2006) 88.
[43] E. Vincent, C.S. Becquart, C. Domain, Nucl. Instrum. Methods. Phys. Res. B 255 (2007) 78.
[44] F. Soisson, C.S. Becquart, N. Castin, C. Domain, L. Malerba, E. Vincent, Atomistic kinetic Monte Carlo studies of microchemical evolution driven by diffusion processes under irradiation 406 (2010) 55.
[45] G.R. Odette, G.E. Lucas, JOM 53 (2001) 18.
[46] A.D. Le Claire, J. Nucl. Mater. 69 and 70 (1978) 70.
[47] A.V. Barashev, A.C. Arokiam, Philos. Mag. Lett. 86 (2006) 321.
[48] A. Hardouin Duparc, A. Barbu, Mater. Res. Soc. Symp. Proc. 439 (1997) 509.
[49] C.A. English, S.R. Ortner, G. Gage, W.L. Server, S.T. Rosinski, ASTM-STP 151 (2001) 1405.
[50] K. Tapasa, A.V. Barashev, D.J. Bacon, Yu.N. Osetsky, J. Nucl. Mater. 361 (2007) 52.
[51] M.S. Daw, M.I. Baskes, Phys. Rev. B 29 (12) (1984) 6443.
[52] S.L. Dudarev, P.M. Derlet, J. Phys.: Condens. Matter 17 (2005) 7097.
[53] P.M. Derlet, S.L. Dudarev, Prog. Mater. Sci. 72 (2007) 299.
[54] G.J. Ackland, S.K. Reed, Phys. Rev. B 67 (2003) 174108.
[55] G.J. Ackland, J. Nucl. Mater. 351 (2006) 20.
[56] L.P. Kadanoff, W. Gotze, D. Hamblen, et al., Rev. Modern Phys. 39 (1967) 395–431.
[57] J.M. Ziman, Principles of the Theory of Solids, Cambridge University Press, 1972 (Chapter 10).
[58] G.J. Ackland, D.J. Bacon, A.F. Calder, T. Harry, Philos. Mag. A 75 (3) (1997) 713.
[59] S. Chiesa, P.M. Derlet, S.L. Dudarev, Phys. Rev. B 79 (2009) 214109.
[60] D. Terentyev, L. Malerba, M. Hou, Phys. Rev. B 75 (2007) 104108.
[61] C. Domain, C.S. Becquart, L. Malerba, J. Nucl. Mater. 335 (2004) 121.
[62] B.L. Eyre, A.F. Bartlett, Philos. Mag. 11 (1965) 261.
[63] M.-C. Marinica, F. Willaime, Solid State Phenom. 129 (2007) 67.
[64] J. Marian, B.D. Wirth, J.M. Perlado, Phys. Rev. Lett. 88 (2002) 255507.
[65] K. Arakawa, M. Hatanaka, E. Kuramoto, K. Ono, H. Mori, Phys. Rev. Lett. 96 (2006) 125506.
[66] D. Terentyev, L. Malerba, T.P.C. Klaver, P. Olsson, J. Nucl. Mater. 382 (2008) 126.
[67] S.L. Dudarev, R. Bullough, P.M. Derlet, Phys. Rev. Lett. 100 (2008) 135503.
[68] Y. Mishin, D. Farkas, M.J. Mehl, D.A. Papaconstantopoulos, Phys. Rev. B 59 (1999) 3393–3407.

[69] Y. Mishin, M.J. Mehl, D.A. Papaconstantopoulos, A.F. Voter, J.D. Kress, Phys. Rev. B 63 (2001) 224106.
[70] A.F. Voter, S.P. Chen, Mater. Res. Soc. Symp. Proc. 82 (1987) 175.
[71] M. Ludwig, D. Farkas, D. Pedraza, S. Schmauder, Modell. Simul. Mater. Sci. Eng. 6 (1998) 19.
[72] E.M. Lopasso, M. Caro, A. Caro, P.E.A. Turchi, Phys. Rev. B 68 (2003) 214205.
[73] G. Simonelli, R. Pasianot, E.J. Savino, Mater. Res. Soc. Symp. Proc. 291 (1993) 567.
[74] R.C. Pasianot, L. Malerba, J. Nucl. Mater. 360 (2007) 118. see also L. Malerba, R.C. Pasianot, SCK-CEN Report, ER-6, February 2006.
[75] G. Bonny, R.C. Pasianot, L. Malerba, Philos. Mag., in press.
[76] R. Kikuchi, Phys. Rev. 81 (1951) 988.
[77] F. Ducastelle, Order and Phase Stability in Alloys, Elsevier Science Publisher B.B., North Holland, 1991.
[78] G. Inden, W. Pitsch, Atomic ordering, in: P. Haasen (Ed.), Phase transformations in materials, VCH, Weinheim, 1991, p. 499 (Chapter 9).
[79] R.C. Pasianot, unpublished.
[80] G. Salje, M. Feller-Kniepmeier, J. Appl. Phys. 48 (1977) 1833.
[81] M. Perez, F. Perrard, V. Massardier, X. Kleber, A. Deschamps, H. De Monestrol, P. Pareige, G. Covarel, Philos. Mag. 85 (2005) 2197.
[82] Y. Nagai, Z. Tang, M. Hasegawa, T. Kanai, M. Saneyasu, Phys. Rev. B 63 (2001) 134110.
[83] C. Dimitrov, A. Benkaddour, C. Corbel, P. Moser, Ann. Chim. France 16 (1991) 319.
[84] P.L. Rossiter, R.A. Jago, Phase transformations in solids, in: T. Tsakalakos (Ed.), Mater. Res. Soc. Symp. Proc., 1984, p. 409.
[85] P.L. Rossiter, P.J. Lawrence, Philos. Mag. A 49 (1984) 535.
[86] K.B. Reuter, D.B. Wiliams, J.I. Goldstein, Metall. Trans. A 20 (1989) 719.
[87] G. Bonny, R.C. Pasianot, L. Malerba, Modell. Simul. Mater. Sci. Eng. 17 (2009) 025010.
[88] G. Bonny, R.C. Pasianot, N. Castin, L. Malerba, Philos. Mag. 89 (2009) 3531.
[89] M. Ruda, D. Farkas, J. Abriata, J. Scripta Mater. 46 (2002) 349–355.
[90] R.A. Johnson, A.C. Damask, Acta Metall. 12 (1964) 443;
R.A. Johnson, G.J. Dienes, A.C. Damask, Acta Metall. 12 (1964) 1215–1224.
[91] C.S. Becquart, J.M. Raulot, G. Bencteux, C. Domain, M. Perez, S. Garruchet, H. Nguyen, Compos. Mater. Sci. 40 (2007) 119–129.
[92] D. Hepburn, G.J. Ackland, Phys. Rev. B 78 (2008) 165115.
[93] K. Levenberg, Quart. Appl. Math. 2 (1944) 164;
D. Marquardt, SIAM J. Appl. Math. 11 (1963) 431.
[94] T.T. Lau, C.J. Först, X. Lin, J.D. Gale, S. Yip, K.J.V. Vliet, Phys. Rev. Lett. 98 (2007) 215501.
[95] M. Müller, P. Erhart, K. Albe, J. Phys.: Condens. Matter 19 (2007) 326220.
[96] P. Olsson, J. Wallenius, C. Domain, K. Nordlund, L. Malerba, Phys. Rev. B 72 (2005) 214119.
[97] A. Caro, D.A. Crowson, M. Caro, Phys. Rev. Lett. 95 (2005) 075702.
[98] T. Seletskaia, Yu.N. Osetsky, R.E. Stoller, G.M. Stock, J. Nucl. Mater. 367–370 (2007) 355.
[99] N. Juslin, K. Nordlund, J. Nucl. Mater. 382 (2008) 143.